

# Planar Gradient Coil Design Using L1 and L2 Norms

Hector Sanchez Lopez<sup>1,2</sup> · Yajie Xu<sup>2</sup> · Pulung Nurtantio Andono<sup>1</sup> · Yan Chang<sup>2</sup> · Xiaodong Yang<sup>2</sup>

Received: 27 March 2018  
© Springer-Verlag GmbH Austria, part of Springer Nature 2018

**Abstract** We present a novel and general formulation for the optimisation of gradient coils, wherein the minimization of the conductor length and the simplicity of construction are two of the main design parameters. The bi-planar gradient coils are intended to be part of a new compact neonatal magnetic resonance imaging (MRI) scanner based on a 0.35 T permanent magnet. It is shown that minimizing the current density vector is equivalent to minimizing the wire length. The gradient coil design involves a convex optimization method where the Euclidian and Manhattan norms of the current density vector are minimized under the field linearity, wire width, force and shielding constraints. The design problem is solved iteratively in order to include the influence of the magnetization of the pole and iron ring over the gradient field linearity. A suite of gradient coils using both norms and resistance minimization are designed and their performances are compared. Gradient coils designed using Euclidian norm show shorter wire length and slightly better performance than that designed using Manhattan norms; however, the presence of straight wires in the current pattern is very convenient for manufacturing purpose.

## 1 Introduction

Magnetic resonance imaging (MRI) necessitates the generation of three strong, linear and orthogonal magnetic field gradients in a diameter spherical volume (DSV) of around 500 mm. The magnetic fields are generated by three independent gradient

---

✉ Yajie Xu  
xuyj@sibet.ac.cn

<sup>1</sup> Department of Biomedical Engineering and Department of Computer Science, Universitas Dian Nuswantoro, Semarang, Indonesia

<sup>2</sup> Suzhou Institute of Biomedical Engineering and Technology, Chinese Academy of Sciences, Suzhou, China

coils usually wrapped around a cylindrical surface and casted in epoxy resin. The coils are constructed using wires or cut thin copper sheets that follow a prescribed current pattern architected to minimize the stored magnetic energy and resistance whilst producing a very linear magnetic field gradient. Low resistance and low stored magnetic energy are both required for ultra-fast sequences such as EPI [1]. A high linearity is necessary to ensure that the magnetic field strength is unique to each point within the sample in the scope of the time-integral of the imaging sequence at play, which is essential in order to avoid geometrical distortions in the resulting images after inverse Fourier transformation [2, 3]. Horizontal whole-body gradient coils are usually actively shielded [4] and force compensated [5] in order to circumvent the generation of eddy currents that produce deleterious image artefacts [6] and in mitigating the acoustic noise generated due to the Lorentz interaction of the main magnetic field with the time-varying gradient coil currents [5].

Gradient coils can be also architected to conform to the parallel plane arrangements and have been extensively used in the past few years in the “open” C-shaped MRI scanners [7–14], where they are fixed to the pole faces of a permanent magnet [15]. Contrary to the whole-body cylindrical coils, planar coils normally do not include active shielding mainly due to the limited space available between the radio frequency (RF) coil and the pole face of the permanent magnet, which usually is made of pure iron. Since the conductivity of the pure iron is relatively high (around  $1.03 \cdot 10^7$  S/m), eddy current are always expected to be induced in the polished face of the pole under the temporal variation of the gradient fields. A grid of low electrically conductive material (eddy device) is usually placed between the gradient coil and the pole face in order to mitigate the induction of eddy currents in the main magnet. Unfortunately, it is not possible to completely shield the main magnet from the time-varying gradient fields, so the main magnet is likely to be a source of leakage eddy currents [16, 17]. The eddy currents in turn are a source of Joule heating and hence possible undesirable frequency shifts may occur due to the temperature increase in the pole ring and passive shims. In addition, the magnetic field produced by the eddy currents opposes the gradient field thereby compromising the spatial quality of the magnetic field produced by the gradient coils [18]. The lack of a secondary shielding coil also limits the possibility of force compensation which is key to mitigate acoustic noise. Although mechanical fixation to the pole face using rubber material may absorb part of the mechanical vibration, the remaining acoustic modes may induce disturbing noise, especially in compact scanners such as the neonatal imager.

Manufacturing cost and simplicity of construction are aspects rarely studied by gradient coil designers in both whole body horizontal and planar gradient coils. The first intent to deal with cost by producing a simplified winding pattern was previously presented with the aim of designing shim coils with minimal power loss [19]. The  $l_1$ -norm of the conductor electrical length was minimized using linear programming, thereby sparse and square-shape current patterns were obtained, but with multi-turns located in the same location; thus bringing some rounding issues. Recently, convex optimization was applied to minimize the  $l_1$ -norm of the current density amplitude, thereby minimizing the coil length using Euclidian distance [20]. Circle-shaped current patterns were obtained and several examples were shown where the  $l_1$ -norm minimization combined with a boundary element method (BEM) produces

compact and smooth coil patterns of superior efficiency compared to those obtained with the conventional resistance minimization approaches [21]. However, computer numerically controlled (CNC) machine is required to accurately groove a plate in order to place the conductor in its place.

We hypothesize in this work that the minimization of the wire length using Euclidian or Manhattan distance, in combination with the minimization of the infinity norm of the current density [22], produces compact and regular shaped coil current patterns that can help solve the aforementioned problems associated with lack of shielding, force balancing and cost of manufacturing of planar gradient coils.

In this study, we present a generalized formulation for gradient and shim coil designs using l1-norm and l2-norm minimization of the conductor electrical length. In particular, the new formulation is applied to the design of a planar gradient coil set for neonatal imaging based on a 0.35 T permanent magnet. A suit of gradient coil designs is explored using both Euclidian and Manhattan distance minimization in order to provide a guidance on the advantages and limitations of both techniques, as well as the expected gains in respect to the conventional resistance minimization approach. Coil performance measured as the ratio  $\frac{z}{L}$  and  $\frac{z}{R}$  and force are compared in order to show the variation from a purely Euclidian/Manhattan minimization relative to the resistance minimization. The coil efficiency  $\eta$  is defined as the ratio between the gradient strength and the operating current.  $R$  and  $L$  are the coil resistance and inductance, respectively. Typical Euclidian and Manhattan coil pattern are shown and two x-gradient coils are selected as possible candidates to be built for a 0.35 T open C-shape neonatal imaging scanner.

Finally, a self-shielded Z-gradient coil and its current pattern are implemented to demonstrate that, even using a single plane coil domain, it is possible to achieve shielding by reducing the residual eddy current [23] to levels smaller than 0.5%. Coils designed using Euclidian minimization show a reduction of the cost by shortening the total wire length, which also suggests a simplicity of construction compared to the pattern designed using resistance minimization.

## 2 Methods

### 2.1 Theory

The Euclidian distance measures the shortest distance between two points or equivalently the length of the shortest path between two points in a continuous space. In contrast, the Manhattan distance measures the length of multiple paths connecting two points along axes at right angles. The Manhattan distance is known also as the ‘Taxi Cab metric’ due to the grid discretization of the space. Given two points  $P_1(x_1, y_1)$  and  $P_2(x_2, y_2)$  located in a plane, the Euclidian and Manhattan distances are defined as  $e_2 = \sqrt{(x_2 - x_1)^2 + (y_2 - y_1)^2}$  and  $e_1 = |x_2 - x_1| + |y_2 - y_1|$ , respectively. The concept of Euclidian distance was recently applied to the design of gradient coils [20], which explains why the current patterns show a compact circular shape as the optimization problem finds the shortest distance between two points. As a result, coils of reduced total conductor length are obtained. We show that it is possible to obtain

general formulations of Euclidian and Manhattan distance optimisation approaches in the design of gradient coils where the surface current density  $\mathbf{J}_i$  is treated as a vector rather than the magnitude of the vector [20].

Let us assume that the coil domain is formed by a discrete set of  $N_e$  triangles of thicknesses  $t$  as described in several previous publications on the inverse boundary element method (IBEM) applied to the design of gradient coils [21, 24–28]. The electrical resistance in the coil domain assuming a resistivity  $\rho$  is defined as:

$$R_{\text{tot}} = \frac{\rho}{t} \sum_i^{N_e} \frac{1}{w_i} \sum_{n=1}^{N_i} l_{n,i}, \tag{1}$$

where  $N_i$  is the number of wires in the triangle  $i$ ,  $w_i$  is the wire width and  $l_{n,i}$  is the length of the wire  $n$  in the triangle  $i$ . The resistance in the triangle  $i$  can be expressed as:

$$R_i = \frac{\rho}{tw_i} \sum_{n=1}^{N_i} l_{n,i}. \tag{2}$$

For completeness, Fig. 1 shows an equivalent representation of Fig. A1 as illustrated in [20]. The unknown stream function  $\varphi_i$  is defined within the node triangle [P,Q,R] and is assumed to be constant within the node in the direction of PQ (i.e. along the thickness of the flat copper wire), thus  $\Delta\varphi_i = \varphi_{iR} - \varphi_{iP}$ .

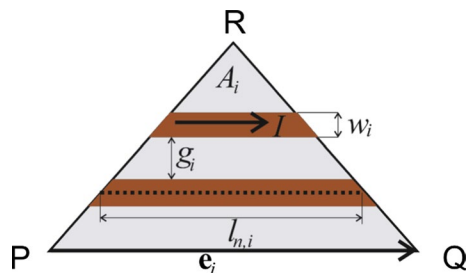
The surface current density in the triangle  $i$  is expressed as follows:

$$\mathbf{J}_i = \frac{\mathbf{e}_i \Delta\varphi_i}{2A_i} \tag{3}$$

and the current that flows in each wire of constant width  $w_i$  is defined by:  $I = \frac{\Delta\varphi_i}{N_i}$ . The total wire length in the triangle  $i$  can then be calculated in the following manner:

$$\sum_{n=1}^{N_i} l_{n,i} = \frac{\|\mathbf{e}_i\|_p N_i}{2}. \tag{4}$$

**Fig. 1** One of the triangles of the coil domain. A constant surface current density  $\mathbf{J}_i$  flows in the triangle  $i$  of area  $A_i$ . A current  $I$  flows in each wire of constant width  $w_i$ , gap  $g_i$  and length  $l_{n,i}$



By combining Eq. (5) and the definition of  $I$  in Eq. (4), we get:

$$\sum_{n=1}^{N_i} l_{n,i} = \|\mathbf{J}_i\|_p \frac{A_i}{I}. \quad (5)$$

Equation (5) implies that the total conductor length in the triangle  $i$  is equivalent to the  $l_p$ -norm of the constant current density  $\mathbf{J}_i$ . This suggests that, if the aim of the optimization problem is to minimize the manufacturing cost by reducing the wire length, then the objective function is expressed as the function of the  $l_p$ -norm of the current density  $\mathbf{J}_i$ .  $p$  can take values of 1 or 2, where  $p=2$  (Euclidian distance) was already presented in [20]. In this work however, Eq. (5) is expressed as function of the current density vector  $\mathbf{J}_i$ , and  $p=1$  (Manhattan distance) is a novel concept presented in this paper.

The total resistance in the coil domain

$$R_{\text{tot}} = \frac{\rho}{I \cdot t} \sum_i^{Ne} \frac{A_i}{w_i} \|\mathbf{J}_i\|_p \quad (6)$$

is obtained by substituting Eq. (5) in Eq. (1). There are two possible variations of Eq. (6) depending on the manufacturing technology to construct the coil winding pattern. If the wire width varies along the coil domain then

$$w_i = \frac{I}{\|\mathbf{J}_i\|_2} \quad (7)$$

and by substituting Eq. (7) in Eq. (6) results in:

$$R_{\text{tot}} = \frac{\rho}{I^2 \cdot t} \sum_i^{Ne} \|\mathbf{J}_i\|_2 A_i \|\mathbf{J}_i\|_p \quad (8)$$

which represents, assuming  $p=2$  a well-known expression of resistance calculation [20]. If the manufacturing technology is based on using wires of constant width for the coil winding, then the minimum wire width is defined as follows:

$$\min w_i = \frac{I}{\|\mathbf{J}_i\|_\infty}. \quad (9)$$

Combining Eqs. (9) and (6) gives:

$$R_{\text{tot}} = \frac{\rho}{I^2 \cdot t} \sum_i^{Ne} \|\mathbf{J}_i\|_\infty A_i \|\mathbf{J}_i\|_p, \quad (10)$$

where  $\|\mathbf{J}_i\|_\infty$  can be replaced by its equivalent form:  $\max \|\mathbf{J}_i\|_2$ . Equations (8) and (10) can be combined in the following convex optimization problem:

$$\text{minimize } \left[ \alpha \varphi^T R \varphi + \beta (1 - \alpha) \sum_i^{Ne} A_i \|\mathbf{J}_i\|_p \right]$$

subject to

$$\frac{((B_z^{\text{coil}} + B_z^{\text{iron}}) - B_z^{\text{target}})_\infty}{\gamma B_z^{\text{target}}_\infty} 100 \leq \varepsilon$$

$$\|\mathbf{J}_i\|_\infty \leq j_0$$

$$\|\mathbf{J}_i^S\|_\infty \leq j_{\text{ring}}$$

$$\|\mathbf{F}_i\|_2 \leq F_{\text{max}}$$

where  $\alpha$  and  $\beta$  are weighting factors,  $B_z^{\text{iron}}$  is any external source of magnetic field, in this case the magnetic field resulting from the magnetization of iron and calculated using the equivalent magnetic charges [14].  $B_z^{\text{target}}$  is the target field with a prescribed spatial behaviour,  $\nu$  is a scaling factor,  $\varepsilon$  the tolerance error of the target field. While the term  $\|\mathbf{J}_i\|_\infty$  can be placed in the objective function multiplied by a weighting factor, in this work it is included as a constraint in order to directly control the desired wire width.  $\mathbf{J}_i^S$  is the induced current density in the first eddy current surface. The infinity norm of  $\mathbf{J}_i^S$  is constrained to values less than  $j_{\text{ring}}$  in order to avoid peak values of the induced current and thereby hot-spots in the pole ring. The values of  $j_0$  and  $j_{\text{ring}}$  can be found in a preliminary iteration and can be adjusted to a desired target.  $\mathbf{F}_i$  is the Lorentz force exerted in each triangle embedded in the magnetic field produced by the main magnet.  $F_{\text{max}}$  is adjusted according to the target value defined by the designer.

The optimization algorithm must be repeated several times. At first  $B_z^{\text{iron}}$  is zero as we have to assume that there is no magnetic field contribution from the pole faces. After the solution of the stream function  $\varphi$  is found, the pole magnetization is calculated [14]. The second iteration includes the magnetic field  $B_z^{\text{iron}}$  produced by the last stream function solution. The process is terminated when the target homogeneity  $\varepsilon$  is fulfilled.

The optimization problem was implemented in Matlab 2016a (The Mathworks, Natick, MA, USA) on a ASUS laptop GX700VO equipped with an Intel® i7-6820HK @ 2.7 GHz and 32 GB of RAM.

## 2.2 The design problem

To demonstrate the new method, we shall design a gradient coil capable of generating at least 40 mT/m in a 165 mm DSV, with a slew rate larger than 150 T/m/s using a power amplifier capable of delivering 150 Amps at 150 V, a total force of less than 30 N and a residual eddy current magnetic field smaller than 0.5%. Figure 2a, shows a schematic representation of the coil domain, DSV, pole and ring, the permanent magnet (PM) and the iron yoke.

The pole and ring were both made of pure iron are considered in the design problem. We assumed that the magnetic field produced by the gradient coil has no significant influence on the permanent magnet (PM) or on the iron yoke magnetization that would influence the magnetic field produced by the coil. The pole and the pole ring were only considered in the design problem. Figure 2b describes the main dimensions of the  $x$ -gradient coil domain as well the dimensions of the pole and ring. The ring is represented in a shaded area and only the surface defined by the coordinates (1,2,3,4) are included as the eddy first surface. The pole ring conductivity was set to  $1.03 \cdot 10^7$  S/m and the relative permeability  $\mu_r$  was 380.

## 2.3 $l_p$ -norm vs resistance minimization

A suit of 16  $x$ -gradient coils were studied using  $l_1$ -norm and  $l_2$ -norm and compared with a conventional resistance minimization to determine the gains and possible limitations of the two  $l_p$ -norm methods. This numerical study was of paramount importance to the neonatal MRI system project as it provided a decisive selection guide for best candidate coils to be manufactured in scope of both, the coil performance and simplicity of construction. The magnetic field influence from the iron pole and ring were considered after the candidate coils were selected.

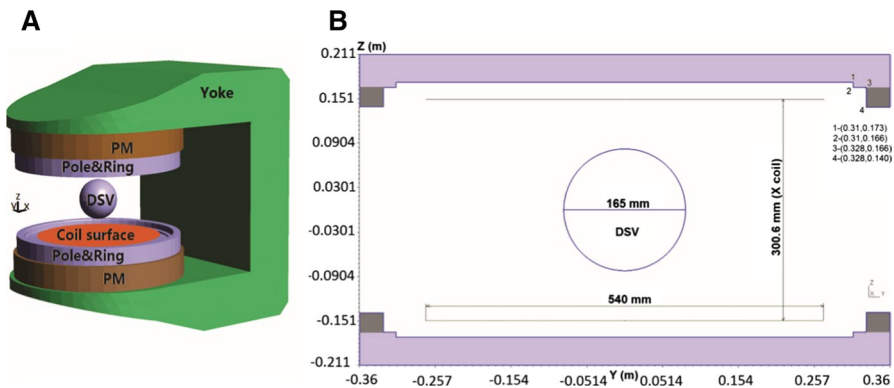


**Fig. 2** Gradient coil design problem. **a** 0.35 T magnet formed by the yoke, permanent magnet, pole and pole ring. **b** A linear magnetic field is prescribed in a 165 mm DSV. The  $x$ -planar coil is placed in parallel planes separated by the distance of 300.6 mm. The coordinates of the pole and ring are provided for completeness. The shaded region represents the first eddy surface

The factor  $\alpha$  was varied in the range 0–1,  $J_0$  was set such that the minimum wire of constant width was equal to 4 mm for all the designs, the wire gap was set to 2.2 mm, the non-linearity tolerance  $\varepsilon$  was constrained to 5% and the residual eddy current smaller or equal to 0.5%. The magnetic field profile generated by the 0.35 T magnet was also provided for an accurate Lorentz force calculation.  $F_{\max}$  was restricted to values no larger than 30 N. The number of contours for all the designs was set to 28.

Best performance  $x$ -gradient coils were selected and an additional optimization was performed this time, including the influence of the pole and ring magnetization. The studied was focused in the  $x$  coil only, as the results in terms of coil performance as function of the applied method is also valid for the  $y$ -coil. Three  $z$ -gradient coils were also designed considering  $\alpha = 1$  and  $\alpha = 0$  to evaluate the coil performance when resistance, l1-norm and l2-norm methods are applied. The  $z$ -gradient coils were designed using l1-norm and l2-norm strategies and considering the pole and ring magnetization and its influence over the gradient coil magnetic field. The wire of constant width was fixed to 3 mm and the gap between wire edges to 2 mm.

### 3 Results

Figure 3 presents the behaviour of the figures of merit (FoMs) that have been calculated in order to characterize the coil performance; Fig. 3a  $\frac{\eta^2}{L}$  and Fig. 3b  $\frac{\eta^2}{R}$ . The first expression in Fig. 3a is related to the ratio between the efficiency and inductance (i.e.  $\frac{\eta^2}{L}$ ) and the second (Fig. 3b) between the coil efficiency and the resistance (i.e.  $\frac{\eta^2}{R}$ ) [29].

The variation of  $\alpha$  in the range from 0 to 1 permits us to study the trade-offs between the  $l_p$ -norm and the conventional resistance minimization. Figure 4a

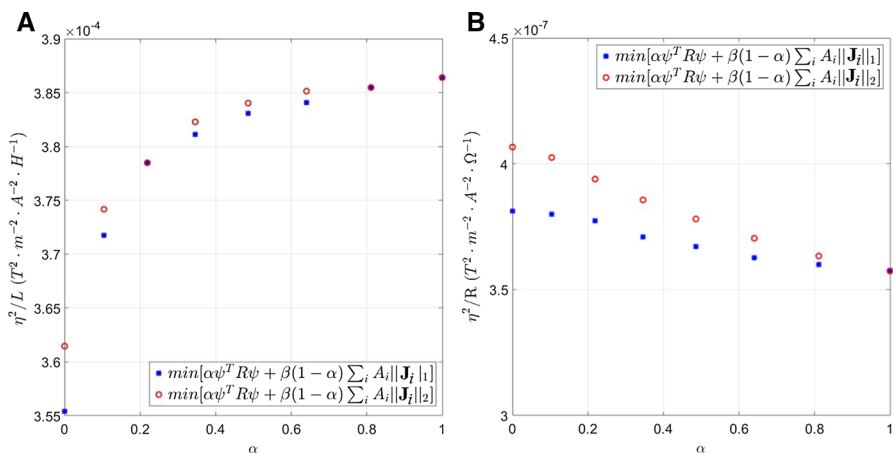


**Fig. 3** Variation of the coil performance from purely  $l_p$ -norm to the conventional resistance minimization. The figure of merits **a**  $\frac{\eta^2}{L}$  and **b**  $\frac{\eta^2}{R}$  provide guidance on the coil performance in terms of the trade-off between  $l_p$ -norm and resistance minimization



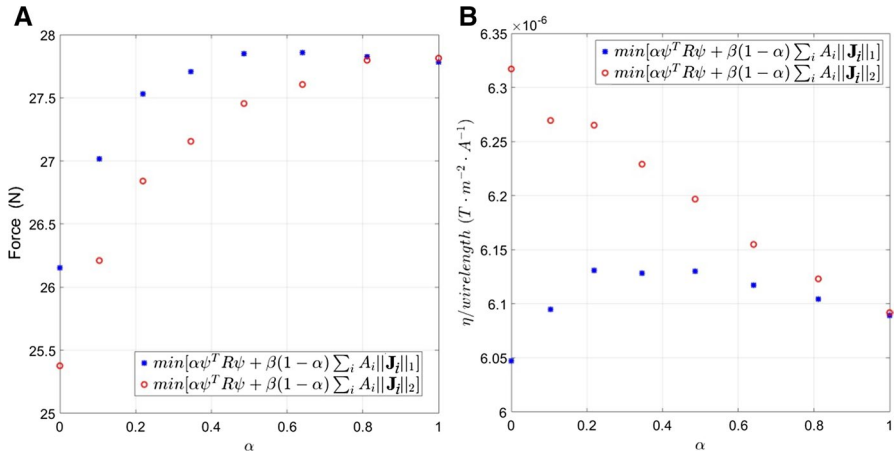


**Fig. 4** **a** Force variation in the *x*-coil as function of the trade-off between *lp*-norm optimization and conventional resistance minimization. **b** The ratio  $\eta$ /wire length guides the coil designer in terms of the manufacturing cost when *lp*-norm strategies are applied as design methods

shows the force exerted in the *x*-coil winding when the coil is embedded in the 0.35 T magnetic field.

Both optimization methods, Manhattan and Euclidian, yield different force behaviours when the *lp*-norm is weighted in respect to the resistance minimization. Figure 4b depicts the ratio between efficiency and conductor length. It intends guide the designer to choose the optimization method on terms of the coil cost by relating the proportion of field strength with wire length.

Figure 5 show the current patterns of the suit of *x*-gradient coils designed considering  $\alpha=0$  and purely *lp*-norm wire length minimization (A and B) and (C) resistance minimization strategy.

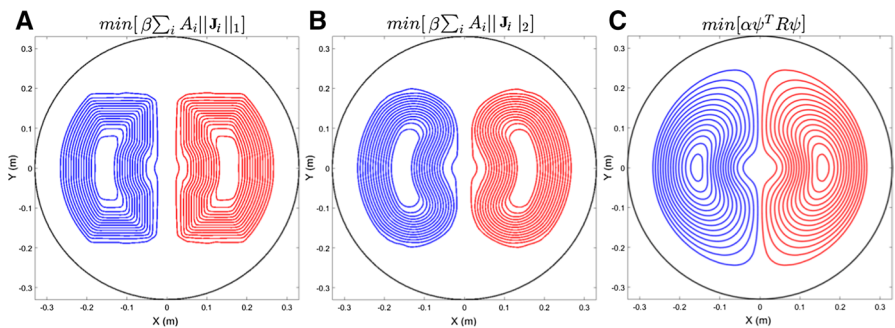


**Fig. 5** Half of the *x*-planar gradient coils for neonatal imaging. **a** D-shape coil designed using the Manhattan minimization (11-norm). **b** Bin-shaped l2-norm coil and the conventional **c** a typical resistance minimization *x*-planar gradient coil. The circle surrounding the coil pattern represents the coordinate (4) in Fig. 2. Different colours indicate opposite current directions

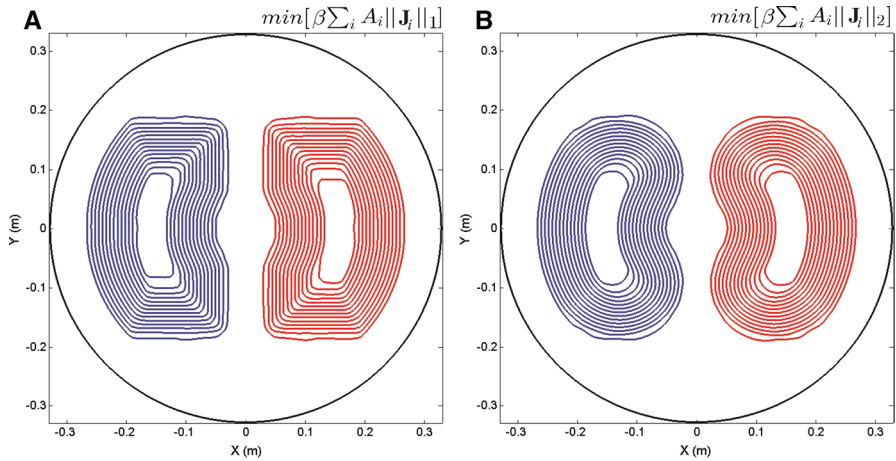


**Fig. 6** **a** Half of the D-shape and **b** Bin-shape  $x$ -gradient coils designed using the Manhattan and Euclidean norms, respectively. Both coils were designed considering the iron pole and ring of the 0.35 T permanent magnet. The circle surrounding the coil pattern represents the coordinate (4) in Fig. 2. Different colours indicate oppose current directions

**Table 1** Characteristics of the designed  $x$ -planar gradient coils. The coils were designed assuming the influence of the pole iron and ring

Properties	Manhattan norm l1-norm	Euclidian norm l2-norm
$\eta$ ( $\mu\text{T}/\text{m}/\text{A}$ )	427	439
Inductance ( $\mu\text{H}$ )	340.4	348
Resistance ( $\text{m}\Omega$ )	184	181
Slew rate ( $\text{T}/\text{m}/\text{s}$ ) @ 150 V	166	168
Rise time ( $\mu\text{s}$ )	226	224
Residual eddy current (%)	0.08	0.078
Max non-linearity DSV ( $16 \times 16 \times 16$ ) (cm)	+ 5/- 3.89%	+ 5/-4.10%
Force (N)	16	15

The black circle surrounding the coil patterns provides a guide on the proximity of the coil current pattern to the inner surface of the pole ring. Figure 5a, b are the first designs based on Fig. 3 when  $\alpha=0$  and Fig. 5c is the design corresponding to Fig. 3 when  $\alpha=1$ .

Figure 6 illustrates the  $x$ -coil assuming  $\alpha=0$  and considering the pole and ring magnetization under the influence of the gradient coil magnetic field. Figure 6a describes a typical Manhattan coil wire pattern while Fig. 6b shows a distinctive Euclidian gradient coil winding shape [20].

Table 1 shows the main characteristics of the gradient coils illustrated in Figs. 6a, b. The second column corresponds to the coil designed using the new

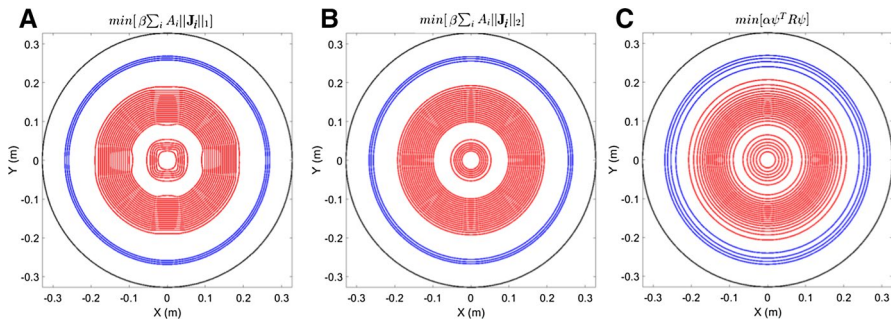


**Fig. 7** Half of the self-shielded z-planar gradient coil designed using **a** Manhattan, **b** Euclidian norms and **c** resistance minimization. The coils are optimized assuming the influence of the iron pole and ring. Different colours indicate opposite current directions

**Table 2** Characteristics of the z-self shielded gradient coils using the generalized norm minimization strategy and the conventional resistance minimization method

Properties	Manhattan l1-norm	Euclidian l2-norm	Resistance minimization
$\eta$ ( $\mu\text{T/m/A}$ )	696	704	648
Inductance ( $\mu\text{H}$ )	355	360	322
Resistance ( $\text{m}\Omega$ )	262	258	282
Slew rate ( $\text{T/m/s}$ ) @ 150 V	268.5	268.5	271
Rise time ( $\mu\text{s}$ )	124.4	124.5	122
Residual eddy current (%)	0.36	0.48	0.47
Max non-linearity DSV ( $16 \times 16 \times 16$ ) (cm)	+ 4.33/- 4.95%	+ 4.25/- 4.81%	+ 4.34/- 5%
Force (N)	11	9.64	11.8

formulation presented in this paper based on l1-norm and the second column presents the values belonging to the coil optimized using Euclidian norm.

Figure 7 shows the half of three z-self-shielded gradient coils. The coils were designed considering the magnetization created by the magnetic field produced by the z coils. Figures 7a, b describe the coils designed with the new l1-norm and the already presented l2-norm [20]. Figure 7c illustrates the case of resistance minimization.

The Table 2 is divided into four columns. The first column represents the coil characteristics, while the second and third columns show the values corresponding to the coils optimized using Manhattan and Euclidian norms. The properties of the coil optimized using the conventional resistance minimization appears in the third column.

Table 3, illustrates the radial positioning of the loops presented in Fig. 7b. The radius has been grouped in three different columns as they are appearing clustered in three sections in Fig. 7b. The ‘Sense’ column is presented in order to account for the current direction in the self-shielded planar coil.

**Table 3** Radius corresponding to each loop in the self-shielded  $z$ -gradient coil optimized using  $l_2$ -norm

Sense	Radius (mm)	Sense	Radius (mm)	Sense	Radius (mm)
+	23.33	+	99.75	-	255.73
+	28.46	+	104.85	-	261.91
+	33.69	+	109.94	-	266.97
+	38.82	+	114.99		
+	43.57	+	120.02		
+	53.47	+	125.09		
		+	130.13		
		+	135.21		
		+	140.23		
		+	145.29		
		+	150.3		
		+	155.35		
		+	160.36		
		+	165.43		
		+	170.52		
		+	175.51		
		+	180.57		
		+	186.08		
		+	192.29		

Axial position  $\pm 148.7$  mm

The coil is shown in Fig. 7b

## 4 Discussion

The new formulation presented in Eq. (6) includes two methods based on the minimization of the total wire length: Manhattan (this paper) and Euclidian norm. Equation (5) shows that the total conductor length can be expressed as the  $l_p$ -norm of the current density vector and therefore the optimization problem can be based on the minimization of  $\|\mathbf{J}_i\|_p$ ; thereby the problem can be setup as a convex optimization method [20]. In this paper the product  $\|\mathbf{J}_i\|_\infty \|\mathbf{J}_i\|_p$  in Eq. (10) was implemented as the minimization of  $\|\mathbf{J}_i\|_p$  in the objective function and  $\|\mathbf{J}_i\|_\infty$  was included as linear constraint. This form provides a direct control of the wire width while the optimization still keeps its convex properties.

Figure 3a shows that the FoM  $\frac{2}{L}$  tends to increase when the design problem is weighted towards the conventional resistance minimization method. The coil patterns designed using resistance minimization tends to expand or cover the total area of the coil domain for an optimal Joule dissipation. The mechanism of spreading the coil pattern yields a significant minimization of the inductance mainly due to the reduction of the turn–turn mutual inductive coupling. In contrast, the minimization of the Manhattan (this paper) and Euclidian norms of the wire length tend to produce compact coil winding and as consequence higher inductance. Therefore, if a coil of very high slew rate is required as part of the design goal, then the resistance minimization is the method of choice. Conversely, if the power dissipation when using a wire of

constant width is the main design target, in this case  $l_p$ -norm minimization should be used. Figure 3b demonstrates that  $l_p$ -norm, and in particular  $l_2$ -norm, show the highest performance  $\frac{z}{R}$  compared to  $l_1$ -norm and resistance optimization.

In terms of force compensation, the Euclidian coil ( $l_2$ -norm) shows the minimal total force. However, the coil designed using resistance minimization tends to be less balanced than that using  $l_p$ -norm optimization. Figure 4a describes the behaviour of the force exerted on the coil winding when the optimization method tends to towards conventional resistance minimization. The force tends to increase as the coil current pattern approaches the pole ring where the magnetic field profile becomes less uniform and more difficult to control. The winding compactness characterizing the  $l_p$ -norm coils favours the force compensation.

Figure 4b demonstrates that the  $l_2$ -norm coil is the better choice if the manufacturing cost is one of the goals of the coil design. The compactness and the tendency of the coil pattern to reduce the wire length by shorting the distance in the Euclidian space yields the best cost effective coil. The  $l_1$ -norm coil shows the lowest cost effective figure as the coil pattern tends to use straight wires, while resistance minimization and  $l_2$ -norm produces smooth current patterns. Figure 5 shows the typical solutions for the three design strategies. As discussed previously, the  $l_1$ -norm (Fig. 5a) tends to produce straight wires as a consequence of the wire length reduction by  $l_1$ -norm minimization, while the  $l_2$ -norm (Fig. 5b) produces bin-shape-type coils of smooth profile. The resistance minimization (Fig. 5c) generates a familiar current topology where the wires tends to occupy the entire coil domain surface. The  $l_2$ -norm is the most cost effective solution, but by visual inspection the D-shape like pattern of the  $l_1$ -norm may indicate some advantages when manual wire placing is used. The sections of straight wires may facilitate the coil construction.

Figure 6a, b describes the selected coils configurations considering the simplicity of construction, force balancing and  $\frac{z}{R}$  performance. The coils were designed assuming the change of the magnetization due the gradient field. As the iron is assumed to be linear, the change in the gradient amplitude manifests as a linear change in the amplitude of the iron magnetization, therefore the linearity of the gradient field is constant for any sequence.

Table 1 shows that both gradient coil efficiencies are better than that of the design target, by about 1.6 and 1.65 times, respectively. That factor is due to the presence of the iron pole and ring that unavoidably increases the inductance by nearly two-fold compared to when the coil is in the absence of the iron pole and ring. The slew rate in both designs outperforms the target values and the  $l_2$ -norm shows slightly higher value to that of the coil conceived with  $l_1$ -norm. Residual eddy currents, linearity and force are all well below the design requirements. In the absence of the iron, the gradient coil non-linearity increases to 8%, which implies that in order to produce a linear field, the effects of the iron pole and ring must be considered.

While the characteristics of both coils do not differ significantly, the winding pattern makes all the difference for the manufacturing process. The  $l_1$ -norm shows a large number of straight wire sections which is significantly preferred over the curved wire sections, especially when manual winding is used to build the  $x$  and  $y$  coils.

Figure 7 illustrates the winding pattern of the self-shielded bi-planar  $z$ -gradient coil. The  $l_p$ -norm  $z$  coils show three clusters of wires; the current changes direction in the most exterior wires. While  $l_1$ -norm coil shows sections of straight wires,

$l_2$ -norm illustrates a smooth circular-shape profile. The  $z$ -coil designed using resistance minimization (Fig. 7c) shows a typical effect of spreading the wires to occupy the whole surface, which effectively reduces the inductance with an undesirable reduction in coil efficiency.

Table 2 illustrates the values of the main characteristics for all three designs. The  $l_p$ -norm coils show smaller resistance than that of the conventional resistance minimization method. This effect was previously documented [20] and is valid when the coil uses wires of constant width. The three reversed turns found close to the iron ring reduce the residual eddy below 0.5% thereby fulfilling the design target. In contrast, the force in the  $z$  coil is lower compared to that in the  $x$  and  $y$  coils.

Under the criteria of simplicity and the presence of sections of straight wires, the gradient coil designed with  $l_1$ -norm was eventually selected for manufacturing. It is however clear that the coil designed using  $l_2$ -norm shows superior performance compared to both  $l_1$ -norm and resistance minimization technique. Table 3 shows the radius of the loops for the  $l_2$ -norm coil for verification and completeness.

## 5 Conclusion

A new and general gradient coil design method based on the minimization of the  $l_p$ -norm of the current density vector has been presented. The formulation covers the case of the  $l_2$ -norm previously presented [20]. The minimization of the wire length is equivalent to the minimization of the  $l_p$ -norm of the current density vector. Gradient coils designed using resistance minimization method are recommended when the slew rate is one of the main design goals. If a conductor of constant width is used and power dissipation is one of the design targets however, then  $l_2$ -norm coil or Euclidian distance minimization is the preferred design choice. If simplicity of construction is the priority, then  $l_1$ -norm is recommended due to the presence of straight wires in the current pattern, even though  $l_2$ -norm may show a better cost effective ratio in terms of gradient strength per wire. While the coils designed using the  $l_p$ -norm and resistance minimization fulfil the requirements for neonatal MRI scanner, the gradient coils designed using  $l_1$ -norm were effectively chosen to be constructed due to the presence of straight wire sections, which can be much easier manufactured with great accuracy.

**Acknowledgements** The authors kindly acknowledge the funding support of Universitas Dian Nuswantoro and NSFC Grant nos. 11505281 and 11675254.

## References

1. F. Schmitt, M.K. Stehling, R. Turner, *Echo-planar imaging: theory, technique and application*. Springer, Berlin, Heidelberg, New York (1998)
2. R. Turner, *Magn. Reson. Imaging* **11**(7), 903–920 (1993)
3. J. Jin, *Electromagnetic analysis and design in magnetic resonance imaging*. CRC press, Boca Raton, 1998
4. P. Mansfield, B. Chapman, *J. Magn. Reson.* **66**(3), 573–576 (1986)

5. D.C. Alsop, T.J., *Magn. Reson. Med.* **35**(6), 875–886 (1996)
6. M.A. Morich, D. Lampman, W. Dannels, F. Goldie, *Med. Imaging IEEE Trans.* **7**(3), 247–254 (1988)
7. M. Martens, L. Petropoulos, R. Brown, J. Andrews, M. Morich, J. Patrick, *Rev. Sci. Instrum.* **62**(11), 2639–2645 (1991)
8. A. Peters, R. Bowtell, *Magn. Reson. Mater. Phys., Biol. Med.* **2**(3), 387–389 (1994)
9. B. Fisher, N. Dillon, T. Carpenter, L. Hall, *Imaging* **15**(3), 369–376 (1997)
10. H. Liu, C.L. Truwit, *Med. Imaging IEEE Trans.* **17**(5), 826–830 (1998)
11. D. Tomasi, E. Caparelli, H. Panepucci, B. Foerster, *J. Magn. Reson.* **140**(2), 325–339 (1999)
12. K. Yoda, *J. Appl. Phys.* **67**(9), 4349–4353 (1990)
13. L.K. Forbes, M.A. Brideson, S. Crozier, *Magnet. IEEE Trans.* **41**(6), 2134–2144 (2005)
14. J. Wang, M.G. Abele, H. Rusinek, *J. Magn. Reson. Imaging* **6**(1), 239–243 (1996)
15. Y. Lai, X. Jiang, G. Shen, *Appl. Supercond. IEEE Trans.* **12**(1), 737–739 (2002)
16. Y. Yao, C.S. Koh, D. Xie, *Magnet. IEEE Trans.* **40**(2), 1164–1167 (2004)
17. T. Miyamoto, H. Sakurai, H. Takabayashi, M. Aoki, *IEEE Trans. Magn.* **25**(5), 3907–3909 (1989)
18. P. Jehenson, M. Westphal, N. Schuff, *J. Magn. Reson.* **90**(2), 264–278 (1969)
19. S.E. Ungersma, H. Xu, B.A. Chronik, G.C. Scott, A. Macovski, S.M. Conolly, *Magn. Reson. Med.* **52**(3), 619–627 (2004)
20. M.S. Poole, Shah N. Jon, *J. Magn. Reson.* **244**, 36–45 (2014)
21. G.N. Peeren, *J. Comput. Phys.* **191**(1), 305–321 (2003)
22. M.S. Poole, P.T. While, H. Sanchez Lopez, S. Crozier, *Magn. Reson. Med.* **68**(2), 639–648 (2012)
23. S. Shvartsman, M. Morich, G. Demeester, Z. Zhai, *Concepts Magnet. Reson. Part B Magnet. Reson. Eng.* **26**(1), 1–15 (2005)
24. S. Pissanetzky, *Meas. Sci. Technol.* **3**(7), 667 (1992)
25. M. Poole, R. Bowtell, *Concepts Magnet. Reson. Part B Magnet. Reson. Eng.* **31**(3), 162–175 (2007)
26. H. Sanchez Lopez, M. Poole, S. Crozier, *J. Magn. Reson.* **199**(1), 48–55 (2009)
27. H. Sanchez Lopez, F. Liu, M. Poole, S. Crozier, *Magnet. IEEE Trans.* **45**(2), 767–775 (2009)
28. C.T. Harris, D.W. Haw, W.B. Handler, B.A. Chronik, *J. Magn. Reson.* **234**, 95–100 (2013)
29. J. Carlson, K. Derby, K. Hawryszko, M. Weideman, *Magn. Reson. Med.* **26**(2), 191–206 (1992)